TAIYO NIPPON SANSO Technical Report No. 43 (2024)

Articles

# Development of Membranes with High Oxygen-Separation Performance at Extremely Low Temperatures

ISHIZAKI Kazutoshi*

A significant amount of oxygen is typically required for various industrial applications. Cryogenic distillation has long been the dominant method for oxygen production due to its ability to yield high-purity oxygen and large production capacity. However, the low relative volatility of the oxygen/argon system has led to a continuous increase in the size of air-separation units (ASUs). In the double-column process, further size reduction of ASUs presents significant challenges. A potential solution is the process intensification of other unit operations in combination with distillation. In this context, membrane-based separation, which allows continuous extraction of products and is not bound to gas–liquid equilibrium, is a promising technology. However, research on separation mechanisms under extremely low temperatures remains limited. In this study, bis(triethoxysilyl)methane (BTESM), a material that enables precise pore-size regulation, was examined, and the separation performance of BTESM membranes was evaluated for oxygen, argon, and nitrogen under low temperatures (around -115 °C) . The results showed that at -115 °C, the BTESM membrane exhibited unprecedented separation performance, with oxygen/argon and oxygen/nitrogen selectivity values of 12.7 and 11.8, respectively, as well as high permeance compared with existing frameworks for the oxygen-selective membranes.

## 1 Introduction

### 1.1 Oxygen Production and Membrane Separation

Oxygen is used in a wide range of industries, with its demand increasing annually 1), 2). Industrial oxygen production is typically performed using air-separation units (ASUs) based on a double-distillation column process, which was developed more than a 100 years ago 3). Distillation is an energy-intensive process, and ASUs are no exception 4). Therefore, industrial gas manufacturers, including our organization, have conducted extensive research to enhance the energy efficiency of ASUs 5), 6), 7). In addition, oxygen production by cryogenic distillation requires large distillation columns to separate the oxygen/argon mixture, characterized by a low relative volatility. This need results in an increase in equipment size. To address these issues, integrating the conventional cryogenic distillation process with a new unit-operation process is desirable.

A promising approach in this context is membrane-based separation, as it does not involve phase changes and is not bound to gas–liquid equilibrium 8). Moreover, the product can be continuously extracted 9). Membrane-based separation of oxygen has been in use for several decades. Since the development of air-separation membranes in 1980 10), organic membranes have been constructed using materials such as hollow fibers and polysulphonic acid 11), 12), 13). However, the organic chains in these organic membranes crystallize at low temperatures, causing thermal oscillation halts and resulting in a significant decrease in gas permeance 14). Consequently, these organic membranes are impractical for cryogenic oxygen separation.

With advancements in material technologies 15), 16), 17), separation membranes composed of cost-effective inorganic materials with high permeance and selectivity have been developed. Although a few studies have focused on gas permeation at low temperatures 18), 19), 20), they do not discuss the separation of argon, a common component of air. The kinetic molecular diameters of oxygen, nitrogen, and argon are extremely similar (Table 1). Thus, to integrate membrane separation with cryogenic distillation for industrial oxygen production, membranes for oxygen separation must exhibit high permeability while maintaining extreme thinness, as well as high selectivity with precise pore-size control at low temperatures. Ionic-electronic conducting materials, such as perovskite, enable selective oxygen permeation and can thus yield high-purity oxygen 21), 22), 23). However, the product flow rate is significantly lower than that of separation membranes with other permeation

Table 1 Specifications of gases

| Molecule | Oxygen | Argon | Nitrogen |
|---|---|---|---|
| Molecule shape | 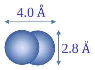 | 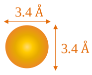 | 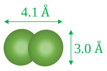 |
| Kinetic diameter [Å] | 3.46 | 3.4 | 3.64 |
| Critical temperature [°C] | −118.2 | −123.2 | −148.2 |
| Standard boiling point [°C] | −195.5 | −185.8 | −182.9 |

---

* Development Division, Cryogenic Separation Technology Development, Tsukuba Development Center, R&D Unit

mechanisms. Furthermore, these solid materials typically operate at temperatures as high as 900 °C, and the product flow rate decreases as the operating temperature decreases. Thus, membranes composed of ionic-electronic conducting materials are unsuitable for integration with cryogenic distillation.

### 1.2 Organosilica Membranes and Research Objective

Silica membranes, composed of inorganic materials, contain dense amorphous pores composed of siloxane bonds, enabling gas separation through molecular sieving. Organosilica membranes [24), 25)], derived from silica membranes, can be fabricated to be extremely thin, with a separation layer as thin as 50 nm, offering high permeation performance. Moreover, these membranes enable structural modifications, such as hydrophilicity/hydrophobicity control and pore-size control using precursors with different carbon numbers, such as bis(triethoxysilyl)methane (BTESM). In addition, owing to their high mechanical strength, attributable to the ceramic components, organosilica membranes are considered promising candidates for low-temperature gas separation.

Considering these aspects, this study was aimed at examining the durability of organosilica membranes with precisely controlled pore sizes at cryogenic temperatures and their ability to permeate and separate oxygen, nitrogen, and argon (characterized by similar kinetic molecular diameters) at low temperatures. The ultimate objective was to achieve process integration of membrane separation with ASUs.

## 2 Experiment

### 2.1 Membrane Fabrication

Figure 1 shows a schematic of the separation membrane. The membrane consists of a porous α-$Al_2O_3$ tube (average pore size 1 μm, outer diameter 10 mm, length 100 mm), onto which the separation layer is coated; and a supporting α-$Al_2O_3$ tube. The membrane has a graded structure in which the porous α-$Al_2O_3$ tube, intermediate layer, and active separation layer are arranged in descending order of pore diameter. The active separation layer is designed to be extremely thin. Both the active separation layer and intermediate layer are BTESM membranes. These membranes are synthesized by the hydrolysis and condensation polymerization of BTESM as the precursor in an alcohol solvent with an acid catalyst to form a sol. This sol is then calcined multiple times in nitrogen or air for 30 minutes within a temperature range of 300 to 600 ℃. Details of membrane preparation can be found in our previous report [26)].

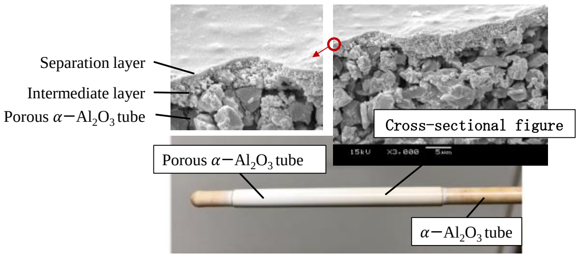

Fig. 1 Schematic of separation membrane

### 2.2 Evaluation of Membrane Pore Size

To quantitatively evaluate the pore size of the fabricated separation membrane, the modified gas translation (GT) model [27), 28)] was used. According to this model, the permeance $P$ can be defined using Equation (1):

$$P = \left(d_p - d_{k,i}\right)\left\{\frac{\left(d_p - d_{k,i}\right)^2}{d_p^2}\right\}\sqrt{\frac{8}{\pi R M_i T}}\frac{\varepsilon}{\tau L} exp\left(-\frac{E_{p,i}}{RT}\right) \qquad (1)$$

where

$P$: Permeance [mol s$^{-1}$ m$^{-2}$ Pa$^{-1}$]

$d_p$: Membrane pore size [m]

$d_{k,i}$: Kinetic diameter of component $i$ [m]

$\varepsilon$: Porosity [-]

$E_{p,i}$: Activation energy of component $i$ [kJ mol$^{-1}$]

$L$ : Membrane thickness [m]

$R$ : Gas constant [J mol$^{-1}$ K$^{-1}$]

$M_i$: Molecular weight of component $i$ [g mol$^{-1}$]

$\tau$: Reflective index [-]

$T$: Absolute temperature [K]

Assuming that component $i$ permeates through Knudsen diffusion, the permeance $P_{i,k}$ of component $i$ can be estimated from the permeance of helium in the membrane, $P_{He}$, using Equation (2):

$$P_{i,k} = P_{He}\sqrt{\frac{M_{He}}{M_i}} \qquad (2)$$

Let $P_i$ denote the measured permeance of component $i$ in the membrane. Then, the dimensionless parameter, normalized Knudsen-based permeance (*NKP*), can be defined as in Equation (3):

$$NKP = \frac{P_i}{P_{i,k}} = \frac{P_i}{P_{He}\sqrt{\frac{M_{He}}{M_i}}} \qquad (3)$$

By substituting Equation (1) into Equation (3) and assuming negligible differences in the activation energies of helium and component $i$, *NKP* can be expressed in a simplified form as in Equation (4):

$$NKP = \frac{P_i}{P_{He}\sqrt{\frac{M_{He}}{M_i}}} = \frac{\left(d_p - d_{k,i}\right)^3}{\left(d_p - d_{k,He}\right)^3} \qquad (4)$$

According to Equation (4), when the permeance values of helium and component *i* are known, the membrane pore size can be theoretically estimated using the membrane pore size $d_p$ as a fitting parameter.

### 2.3 Single and Binary Gas Permeation Experiments

Figure 2 schematically illustrates the gas permeation equipment, including high-purity gas cylinders (He, $H_2$, $O_2$, Ar, $N_2$, $CH_4$, $CF_4$, and $SF_6$), mass flow controllers (FCON 1000 series, 2 L/min), a heat exchanger, a separation membrane, Freon for gas cooling (AGC AK-225G, freezing point -130 °C to -115 °C), liquid nitrogen, a gas chromatograph (Shimadzu GC-6A :TCD for GL Sciences column), and soap film meters (HORIBA SF-U series, 0.2 to 1000 mL). The feed-gas flow rate was controlled according to the experimental conditions using the mass flow controller. The feed gas was desiccated in the drying tube and cooled using Freon before being supplied to the separation membrane. Notably, Freon was cooled using liquid nitrogen via a heat exchanger. The upstream pressure was controlled using a back pressure valve on the retentate side, and the downstream pressure was maintained at atmospheric level. The flow rate and composition of the gas on both the retentate and permeate sides were measured using soap film meters and gas chromatography. For tests at temperatures ranging from room temperature (around 25°C) to 200 °C, the feed-gas temperature was controlled using a mantle heater.

## 3 Results and Discussion

### 3.1 Membrane Durability at Low Temperatures

Figure 3 shows the temperature dependence of helium permeance of the BTESM membrane over a range of -130 °C to 200 °C. Even the permeance values at low temperatures, near -130 °C, were located on the extrapolated line of the permeance at room temperature. This observation suggests that the membrane underwent no deterioration or structural damage at low temperatures. Fig. 4 shows the kinetic diameter dependence of the gas permeance of the BTESM membrane at 200 °C, before and after cooling to -130 °C. Repeated thermal cycling between -130 °C and 200 °C did not influence the permeance of the BTESM membrane across all tested gases. These results indicate that the BTESM membrane exhibits excellent structural stability over a wide temperature range, including at low temperatures.

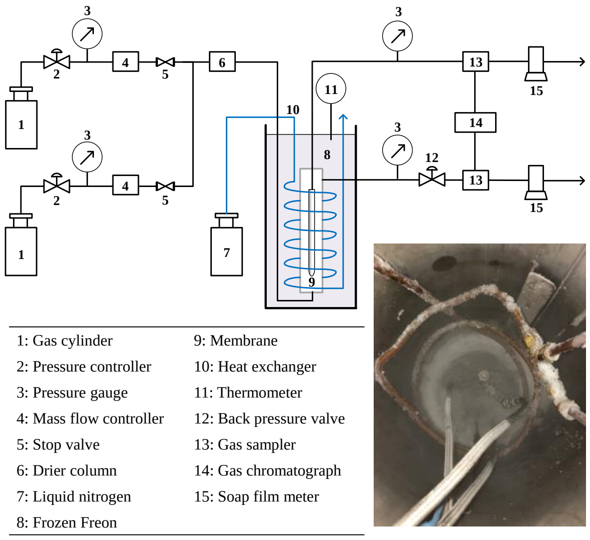

Fig. 2 Schematic of gas permeation test equipment (Inset: Photograph of gas cooling)

### 3.2 Evaluation of Membrane Pore Distribution and Pore Size Control

Figure 5 shows the kinetic diameter dependence of dimensionless gas permeance (normalized to helium permeance at 200 °C) for four membranes fabricated under different calcination conditions (temperature and atmosphere). The solid

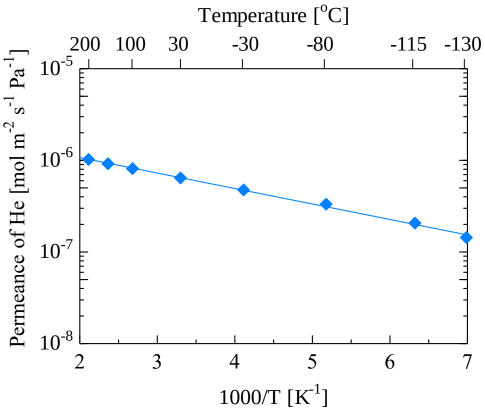

Fig. 3 Temperature dependence of helium permeance of BTESM membrane from -130 °C to 200 °C

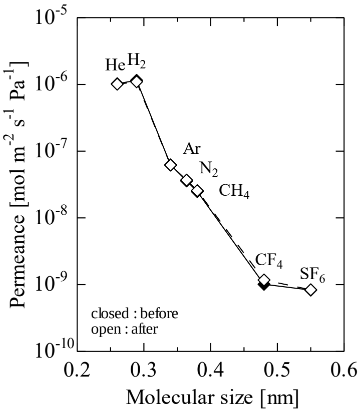

Fig. 4 Kinetic diameter dependence of gas permeance of BTESM membrane at 200 °C, before and after cooling to -130 °C

black line (without symbols) represents the dimensionless permeance calculated based on helium permeance as a reference, assuming that each gas permeates through Knudsen diffusion. A larger deviation from the solid black line indicates enhanced gas selectivity through molecular sieving. Membranes A to C exhibited reduced permeance for gases with larger kinetic diameters, such as $CF_4$ and $SF_6$, compared with $N_2$ and $CH_4$, suggesting a well-defined pore size distribution.

Membrane C exhibited high $N_2$/$CH_4$ selectivity, indicating that its pore size distribution was suitable for molecular sieving around the kinetic diameters of $N_2$ and $CH_4$. One possible reason for this optimization is that the calcination atmosphere was air in this case. In general, owing to the presence of Si–$CH_2$–Si linkages, organosilica membranes form relatively uniform pore sizes while suppressing grain boundaries. However, they are also likely to exhibit large pores. In contrast, owing to the presence of Si–OH groups, silica membranes can form dense pores capable of separating helium and hydrogen, characterized by small kinetic diameters. However, silica membranes typically exhibit a bimodal structure consisting of a dense network and grain boundaries. For the BTESM membrane calcined in air at 500 °C, the condensation of Si–OH groups and partial oxidation of the Si–$CH_2$–Si unit were moderately accelerated. Thus, the high selectivity of the BTESM membrane was likely attributable to the synergistic effect of the uniform pore size formation and grain boundaries suppression associated with organosilica membranes and the formation of dense pores with high molecular sieving effect associated with the silica membrane.

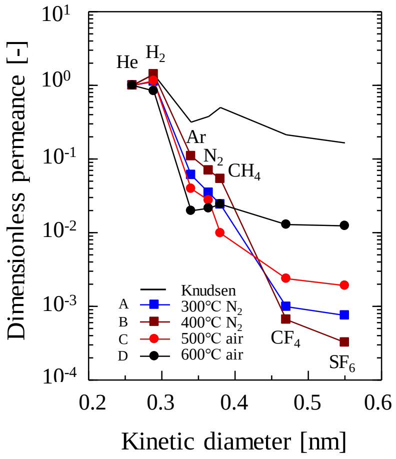

Fig. 5 Kinetic diameter dependence of dimensionless gas permeance (normalized to helium permeance at 200 °C) for BTESM membranes fabricated under different calcination conditions

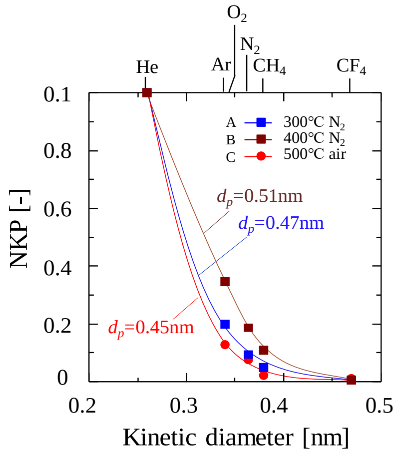

Fig. 6 Kinetic diameter dependence of normalized Knudsen-based permeance for BTESM membranes calcined under different temperatures and atmospheres

In contrast, Membrane D, calcined at 600 °C in an air atmosphere, exhibited a selectivity comparable to that of Knudsen diffusion for gases with kinetic diameters larger than argon. At this higher calcination temperature, most of the carbon groups in the organosilica membrane were likely oxidized, and the membrane was transformed into a silica-like membrane (bimodal structure with dense network and grain boundaries). Thus, Membrane D was unlikely to achieve high oxygen separation performance and subsequent analyses focused on Membranes A, B, and C. **Fig. 6** shows the pore size distributions of Membranes A, B, and C, determined using the modified GT model described in Section 2.2. The results demonstrate that the pore sizes of the three membranes could be precisely controlled through the calcination conditions.

### 3.3 Single Gas Permeation Experiments

Figure 7 shows the feed-pressure dependence of dimensionless gas permeance (normalized to the gas permeance at 200 kPa) of membranes A, B, and C at -115 °C for oxygen, argon, and nitrogen. A previous study [26)] reported that the permeance did not depend on the pressure at a permeation temperature of 30 °C. However, in this study, pressure dependence was observed at -115 °C for all pore sizes and gas species. This phenomenon could be explained by the fact that as the feed pressure increased at low temperatures, the gas formed a dense phase within the membrane pores, similar to condensation, resulting in self-permeation inhibition. The decrease in oxygen permeance was consistent at all pore sizes. However, the decrease in argon and nitrogen permeance became less pronounced as the pore size decreased. This observation suggests that as the pore size decreases, argon and nitrogen exhibit limited diffusion into the pore. Considering the result of single gas permeation experiments conducted using membrane

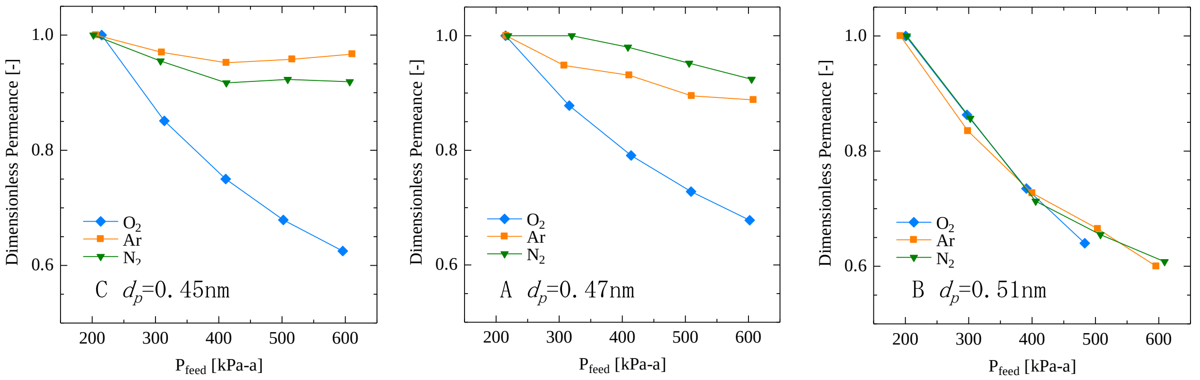

Fig. 7 Feed-pressure dependence of dimensionless gas permeance (normalized to gas permeance at 200 kPa) for oxygen, argon, and nitrogen at -115 °C (From left to right: Membranes C, A, and B)

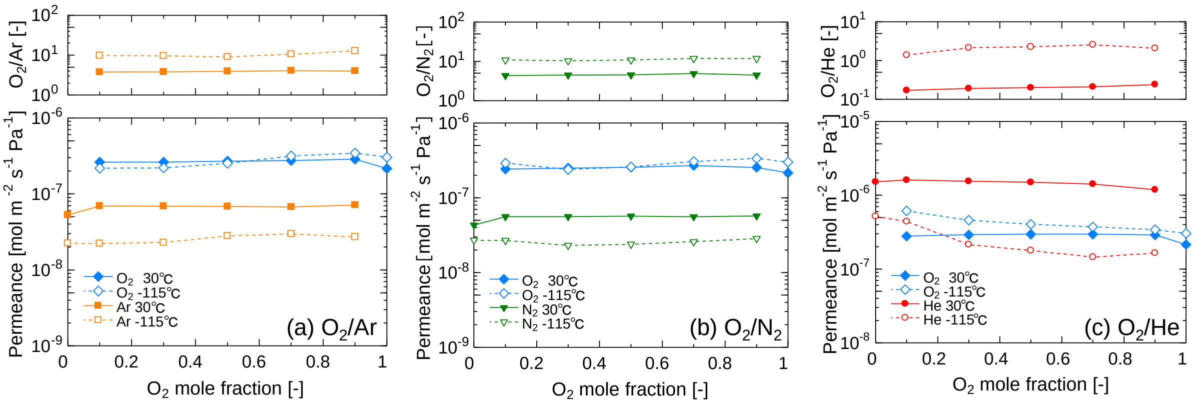

Fig. 8 Effect of oxygen mole fraction on the feed side on gas permeance and oxygen selectivity at 30 °C and -115 °C for BTESM membrane C
(From left to right: oxygen/argon, oxygen/nitrogen, and oxygen/helium gas mixtures)

C, high selectivity is expected in binary separation experiments at low temperatures, unlike that of molecular sieving in the gaseous phase at room temperature. This is attributable to the formation of a selective dense phase composed only of oxygen, which physically inhibits the permeation of other components.

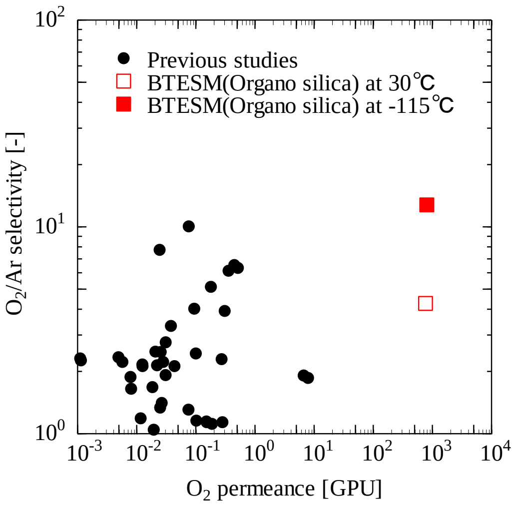

Fig. 9 Comparison of $O_2$/Ar separation performance of existing frameworks and proposed BTESM membrane
(Black: previous studies, Red: this study)

### 3.4 Binary Separation Properties of the BTESM Membrane

Figure 8 shows the gas permeance at 30 °C and -115 °C as a function of the oxygen mole fraction for oxygen/argon, oxygen/nitrogen, and oxygen/helium gas mixtures. These experiments were based on Membrane C, identified in Section 3.3 as having high oxygen selectivity. At 30 °C, the oxygen selectivities for the oxygen/argon and oxygen/nitrogen gas mixtures were 4 and 4.5, respectively. However, at -115 °C, these values increased to 12.7 and 11.8, representing a significant enhancement in membrane performance compared with that at room temperature. The permeance of oxygen, argon, and nitrogen did not depend on the oxygen mole fraction of the feed gas. In terms of the separation of the oxygen/helium gas mixture, helium exhibited preferential permeation at 30 °C. However, at -115 °C, oxygen, with a large kinetic molecular diameter, became the preferentially permeating component. This shift may be attributable to the formation of a dense oxygen phase at low temperatures (as discussed in Section 3.3), which inhibited the permeation of coexisting components. Figs. 9 and 10 present a comparison of oxygen/argon and oxygen/nitrogen separation performance of existing membranes [29), 30), 31)] and the proposed

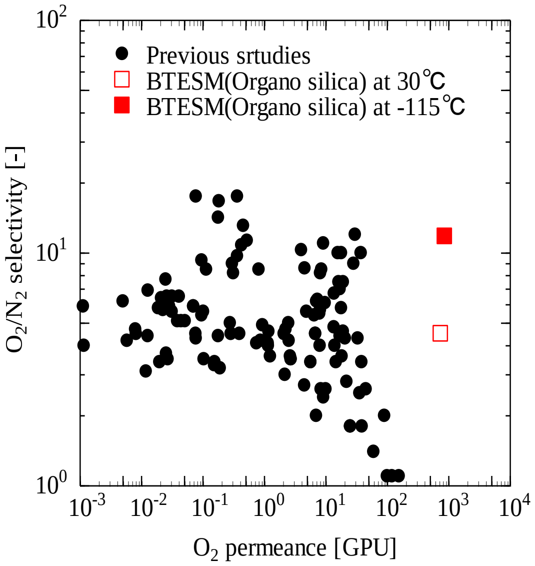

Fig. 10 Comparison of $O_2/N_2$ separation performance of existing frameworks and proposed BTESM membrane
(Black: previous studies, Red: this study)

BTESM membrane. The proposed BTESM membrane achieved higher permeance and greater selectivity for both mixtures compared with the existing membranes, as indicated by its values lying on the right side (horizontal axis, permeance) and upper region (vertical axis, selectivity). These findings confirm that the BTESM membrane demonstrates excellent oxygen permeation and selectivity, representing a promising candidate for oxygen separation.

## 4 Conclusion

BTESM membranes, a type of organosilica membrane that enables diverse structural designs among inorganic membranes, were fabricated, and their oxygen permeation mechanisms at cryogenic temperatures were evaluated. The following conclusions were derived:

- The BTESM membrane did not undergo structural damage or pore blockage at cryogenic temperature.
- By modifying the temperature and calcination atmosphere, the pore size of the membrane could be precisely controlled. In particular, calcination at 500 °C in an air atmosphere resulted in a uniform yet dense separation pore structure with suppressed grain boundaries, resulting in high separation performance.
- By promoting the formation of dense oxygen phases through precise pore size control, the oxygen selectivities for oxygen/argon and oxygen/nitrogen mixtures reached 12.7 and 11.8, respectively, considerably higher than those reported in previous studies. In addition to the oxygen selectivity, the permeance of the proposed membrane was superior to that of existing membranes.

## 5 Future Prospects

Studies on membrane permeation mechanisms at low temperatures remain limited, regardless of the membrane material or separation system. This is primarily because only a small number of industrial fields handle cryogenic environments with market competitiveness. Besides organosilica membranes, which were the focus of this study, there remains significant room for the development of membrane separation technologies at cryogenic temperatures. For example, future work can be aimed at examining membranes based on materials having a high affinity for specific components, evaluating membrane operation under different pressures and temperatures, and identifying methods for integrating membrane separation with distillation. We aim to contribute to the development of innovative separation technologies by leveraging our expertise in technologies operating at cryogenic temperatures, including cryogenic distillation.

References

1) H.-W. Haring, Industrial gases processing, Wiley-VCH Verlag GmbH & Co. KGaA, Weinheim (2008).
2) A. Gorak, H. Schoenmakers, Distillation: Operation and applications, Elsevier, Milton Keynes (2014).
3) F. G. Kerry, Industrial gas handbook Gas: Separation and purification, CRC Press, New York (2016).
4) D. S. Sholl, R. P. Lively, Seven chemical separations to change the world, Nature 532 (2016) 435–437.
5) X.-B. Zhang, J.-Y. Chen, L. Yao, Y.-H. Huang, X.-J. Zhang, L.-M. Qiu, Research and development of large-scale cryogenic air separation in China, J. Zhejiang Univ. Sci. A 15 (2014) 309–322.
6) H. Klein, P. Fritsch, P. Haider, R. Kender, F. Robler, S. Rehfedlt, P. Freko, R. Hoffmann, I. Thomas, B. Wunderlich, Flexible operation of air separation unit, ChemBioEng Rev. 8 (2021) 357–374.
7) M. Tamura, History of air separation unit technologies developed by TNSC, Taiyo Nippon Sanso Technical Report (2022).
8) J. L. Humphrey, G. E. Keller, Separation process technology, McGraw-Hill, New York (1997).
9) C. Castel, E. Favre, Membrane separations and energy efficiency, J. Membr. Sci. 548 (2018) 345–357.
10) J. M. S. Henis, M. K. Tripodi, Multicomponent membranes for gas separations, U.S. Patent 4,230,463 (1980).
11) T. Chung, A review of microporous composite polymeric membrane technology for air-separation, Polym. Polym. Compos. 4 (1996) 269–283.
12) H. M. S. Lababidi, Air separation by polysulfone hollow fiber membrane permeators in series: Experimental and simulation results, Chem. Eng. Res. Des. 78 (2000) 1066–1076.
13) E. Kianfar, V. Cao, Polymeric membranes on base of polymethyl methacrylate for air separation: A review, J. Mater. Res. Technol. 10 (2021) 1437–1461.
14) K. Okamoto, M. Fuji, S. Okamyo, H. Suzuki, K. Tanaka, H. Kita, Gas permeation properties of poly(ether imide) segmented copolymers, Macromolecules 28 (1995) 6950-6956.
15) Y. Shindo, T. Hakuta, H. Yoshitome, H. Inoue, Separation of three-component gas mixture by means of a microporous glass membrane with cocurrent flow, J. Chem. Eng. Jpn. 18 (1985) 485–489.
16) S. Haider, A. Lindbråthen, J. A. Lie, M. B. Hägg, Carbon membranes for oxygen enriched air–Part I: Synthesis, performance and preventive regeneration, Sep. Purif. Technol. 204 (2018) 290–297.
17) C. Y. Chuah, K. Goh, T. H. Bae, Enhanced performance of carbon molecular sieve membranes incorporating zeolite nanocrystals for air separation, Membranes 11 (2021) 1–14.
18) P. Ye, E. Sjöberg, J. Hedlund, Air separation at cryogenic temperature using MFI membranes, Micropor. Mesopor. Mater. 192 (2014) 14–17.
19) P. Ye, D. Korelskiy, M. Grahn, J. Hedlund, Cryogenic air separation at low pressure using MFI membranes, J. Membr. Sci. 487 (2015) 135–140.
20) P. Ye, M. Grahn, D. Korelskiy, J. Hedlund, Efficient separation of $N_2$ and He at low temperature using MFI membranes, AIChE J. 62 (2016) 2833–2842.
21) W. Li, J. Sunarso, Y. Yang, Y. Chen, C. Ge, W. Wang, Y. Guo, R. Ran, W. Zhou, Strategies for improving oxygen ionic conducting in perovskite oxides and their practical applications, Energy. Rev. 3 (2024) 100085.
22) Y. Lu, H. Zhao, X. Chang, X. Du, K. Li, Y. Ma, S. Yi, Z. Du, K. Zheng, K. Swierczek, Novel cobalt-free $BaFe_{1-x}Gd_xO_{3-\sigma}$ perovskite membranes for oxygen separation, J. Mater. Chem. A. 4 (2016) 10454–10466.
23) X. Zhang, J. Motuzas, S. Liu, J. C. Diniz da Costa, Zinc-doped BSCF perovskite membranes for oxygen separation, Sep. Purif. Technol. 189 (2017) 399–404.
24) T. Tsuru, Silica-based membranes with molecular-net-sieving properties: Development and applications, J. Chem. Eng. Jpn. 51 (2018) 713–725.
25) S. O. Lawal, M. Kanezashi, A brief overview of the microstructural engineering of inorganic-organic composite membranes derived from organic chelating ligands, Membranes. 13 (2023) 1–34.
26) R. Izumi, N. Moriyama, K. Ishizaki, H. Nagasawa, T. Tsuru, M. Kanezashi, Gas permeation properties of bridged-type organosilica membranes at extremely low temperatures and the application to oxygen separation, J. Membr. Sci. 691 (2024) 122228.
27) J. Xiao, J. Wei, Diffusion mechanism of hydrocarbons in zeolites—I. Theory, Chem. Eng. Sci. 47 (1992) 1123–1141.
28) A. B. Shelekhin, A. G. Dixon, Y. H. Ma, Theory of gas diffusion and permeation in inorganic molecular-sieve membranes, AIChE J. 41 (1995) 58–67.
29) M. Ceylan, Design and optimization of membrane-assisted distillation processes for argon production from air, Manchester University in the Faculty of Science and Engineering (2019).
30) K. Haraya, S.-T. Hwang, Permeation of oxygen, argon and nitrogen through polymer membranes, J. Membr. Sci. 71 (1992) 13–27.
31) J. Wang, Z. Shi, Y. Zang, H. Jia, M. Teraguchi, T. Kaneko, T. Aoki, Macromolecular design for oxygen/nitrogen permselective membranes—Top-performing polymers in 2020, Polymers 13 (2021) 3012.